J Mater Sci (2011) 46:5581–5586
DOI 10.1007/s10853-011-5508-6

Preparation and photoluminescence properties of Y_2O_3:Eu, Bi phosphors by molten salt synthesis for white light-emitting diodes

Xiaoyong Wu · Yujun Liang · Rui Chen · Mingyu Liu · Yongzhou Li

Received: 19 December 2010 / Accepted: 23 March 2011 / Published online: 14 April 2011

Abstract Y_2O_3:Eu, Bi red phosphors were first prepared by molten salt synthesis (MSS) method at a low temperature. X-ray diffraction (XRD), scanning electron microscopy (SEM), and fluorescence spectrophotometer were used to characterize the as-synthesized phosphors. The results show that as-obtained Y_2O_3:Eu, Bi phosphors have good cubic crystallinity, presenting octahedral morphology with smooth surface and relatively uniform particle size. Bi^{3+} ion as a sensitizer plays a significant effect on the emission intensity of Y_2O_3:Eu, Bi by energy transfer from Bi^{3+} to Eu^{3+} and the optimal concentration of Bi^{3+} is 1.5 mol%. Y_2O_3:Eu, Bi emits excellent red light as the excitation wavelength is between 330 and 420 nm or excited by 254, 466 nm. Meanwhile, its emission intensity is as strong as that of sample prepared by solid-state reaction. So the as-fabricated red phosphors by MSS method would have a promising application in the area of white light-emitting diodes.

Introduction

White light-emitting diodes (LEDs) as the so-called fourth generation solid-state light have attracted considerable attention in recent years because of their extensive applications in display areas based on their excellent characteristics, such as small volume, long lifetime, high energy efficiency, energy-saving, and environment friendly [1–5]. Nowadays, there are two approaches to obtain white LEDs. One approach to produce white light is the combination of blue InGaN chip (450–470 nm) with YAG:Ce yellow phosphor. However, this type of white LEDs has a drawback due to the color deficiency in the red region. In order to solve this problem, a red phosphor, which should be excited by blue InGaN chip effectively, is needed to compensate for the red deficiency of output light [6–8]. The second approach of achieving white light, which is the most promising method, is to use a UV LED chip (350–410 nm) to pump red, green, and blue light-emitting phosphors [9, 10]. This kind of white LEDs has no problem in color deficiency, but red light-emitting phosphor for white LEDs is still limited to the Y_2O_2S:Eu which has several drawbacks in terms of poor efficiency and instability [11, 12]. Therefore, it is an urgent need to develop superior red phosphors for these two types of white LEDs.

In order to meet the requirements of white LEDs for red phosphors, Y_2O_3:Eu, Bi as a promising red phosphor has been reported in several articles [13–16], due to its high efficiency, stability, and appropriate excitation wavelengths for white LEDs. Nevertheless, the preparation of Y_2O_3:Eu, Bi samples in these articles were all in high temperature. It is not only energy consuming but also difficult to control the doping concentration of Bi^{3+} ions because of volatilization of Bi_2O_3 in high temperature [17]. Molten salt synthesis (MSS) as a low temperature method has several advantages over other methods such as good particle size, special morphology, lower sintering temperature, and smooth surface as well as being easy to control properties of resulting particles by adjusting the reaction conditions. In this article, MSS has been first employed to

X. Wu · Y. Liang
Engineering Research Center of Nano-Geomaterials of Ministry of Education, China University of Geosciences, Wuhan 430074, People's Republic of China

X. Wu · Y. Liang (✉) · R. Chen · M. Liu · Y. Li
Faculty of Materials Science and Chemical Engineering, China University of Geosciences, Wuhan 430074, People's Republic of China
e-mail: yujunliang@sohu.com

fabricate Y_2O_3:Eu, Bi phosphors at a low temperature, which is beneficial to co-dope appropriate Bi^{3+} ions into Y_2O_3:Eu correctly. Meanwhile, the role of Bi^{3+} ions in Y_2O_3:Eu sample and the effect of Bi^{3+} concentrations on luminescence properties of Y_2O_3:Eu have been investigated. Some luminescence mechanisms are also discussed.

Experimental

$Y_{2-2x}Eu_{2x}O_3$, $Y_{2-2y}Bi_{2y}O_3$, $Y_{1.86-2y}Eu_{0.14}Bi_{2y}O_3$ ($x = 0.01$, 0.03, 0.05, 0.07, and 0.09; $y = 0.005$, 0.010, 0.015, 0.020, and 0.025) were prepared by MSS. The starting materials were Y_2O_3 (99.99%), Eu_2O_3 (99.99%), Bi_2O_3 (A. R.), KNO_3 (A. R.), and $NaNO_3$ (A. R.). An appropriate stoichiometric ratio of Y_2O_3, Eu_2O_3, and Bi_2O_3 were converted into their nitrates by dissolving in a minimum amount of diluted nitric acids. Then the as-prepared precursors were homogeneously mixed with eutectic mixtures of KNO_3–$NaNO_3$ by milling in an agate mortar. Finally, the homogenous mixture materials were annealed at 550 °C for 5 h and after repeatedly washing and drying, the as-expected $Y_{2-2x}Eu_{2x}O_3$, $Y_{2-2y}Bi_{2y}O_3$, $Y_{1.86-2y}Eu_{0.14}Bi_{2y}O_3$ products were synthesized. For the purpose of comparison, $Y_{1.83}Eu_{0.14}Bi_{0.03}O_3$ and $Y_{1.86}Eu_{0.14}O_3$ were prepared by conventional solid-state reaction (SSR). Y_2O_3, Eu_2O_3 or Eu_2O_3, and Bi_2O_3 were mixed in stoichiometric amounts and H_3BO_3 was added to decrease the firing temperature. Then the powder was calcined at 1300 °C for 4 h under an ambient atmosphere. After cooling down to room temperature in the furnace, the as-heated samples were ground and washed before drying in an oven at 100 °C for 2 h.

The crystal structures of products were recorded with Japan D/Max-3B X-ray powder diffraction (XRD) with Cu Kα ($\lambda = 1.5418$ Å) radiation generated at 30 kV/30 mA. The morphology was studied with Japan JSM-35CF environmental scanning electron microscope (SEM). Photoluminescence was investigated with a FLUOROMAX-4 fluorescence spectrophotometer equipped with a Xe-arc lamp at room temperature.

Results and discussion

The powder XRD patterns of $Y_{1.86}Eu_{0.14}O_3$, $Y_{1.99}Bi_{0.01}O_3$, and $Y_{1.85}Eu_{0.14}Bi_{0.01}O_3$ samples are shown in Fig. 1. According to JCPDS card 25-1011, $Y_{0.90}Eu_{0.10}O_3$ has a cubic crystal structure with the Ia3 (206) space group, and its lattice parameter is 1.061 nm. From Fig. 1, it can be clearly seen that all peaks and relative intensities are well indexed with standard card of $Y_{0.90}Eu_{0.10}O_3$, and no characteristic peaks are observed for other impurities, indicating that the doped Eu^{3+} and Bi^{3+} ions substituted

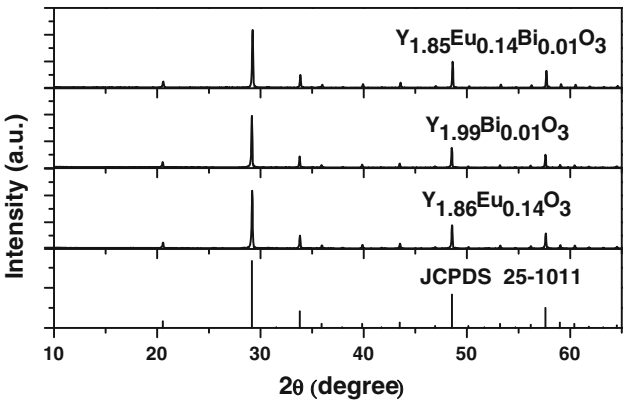

Fig. 1 XRD patterns of as-prepared $Y_{1.86}Eu_{0.14}O_3$, $Y_{1.99}Bi_{0.01}O_3$, and $Y_{1.85}Eu_{0.14}Bi_{0.01}O_3$ samples and standard card of $Y_{0.90}Eu_{0.10}O_3$ (JCPDS 25-1011)

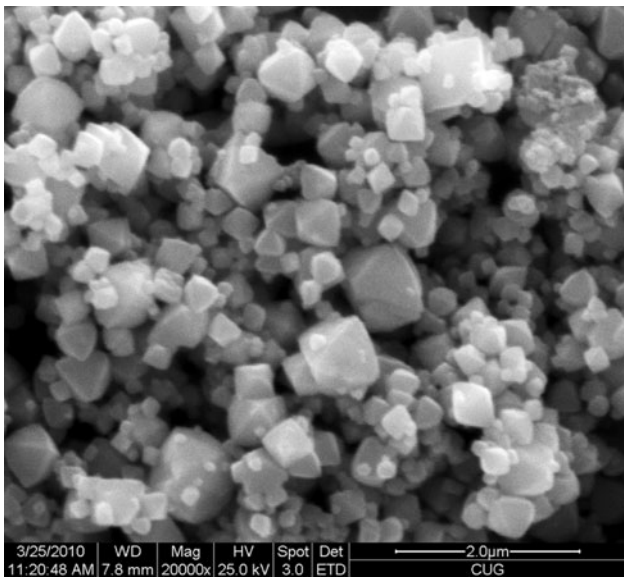

Fig. 2 SEM image of $Y_{1.85}Eu_{0.14}Bi_{0.01}O_3$ calcined at 550 °C for 5 h

Y^{3+} sites have little influence on the host structure. On the other hand, the XRD results mean that $Y_{1.86}Eu_{0.14}O_3$, $Y_{1.99}Bi_{0.01}O_3$, and $Y_{1.85}Eu_{0.14}Bi_{0.01}O_3$ phosphors have been successfully prepared by MSS method at a low temperature.

Figure 2 shows SEM image of as-fabricated $Y_{1.85}Eu_{0.14}Bi_{0.01}O_3$ sample. It is obviously observed that the sample present octahedral morphology with smooth surface as well as relatively uniform particle size, and the particle size is in the range of 100–300 nm except for a few large particles. The formation of special morphology of $Y_{1.85}Eu_{0.14}Bi_{0.01}O_3$ in the MSS method is mainly due to growth mechanism. Cahn [18] advanced that the shape of particles depends on growth mechanism, and his research indicated that if the growth process of particles is controlled by proliferation mechanism, particles reveal spherical shape.

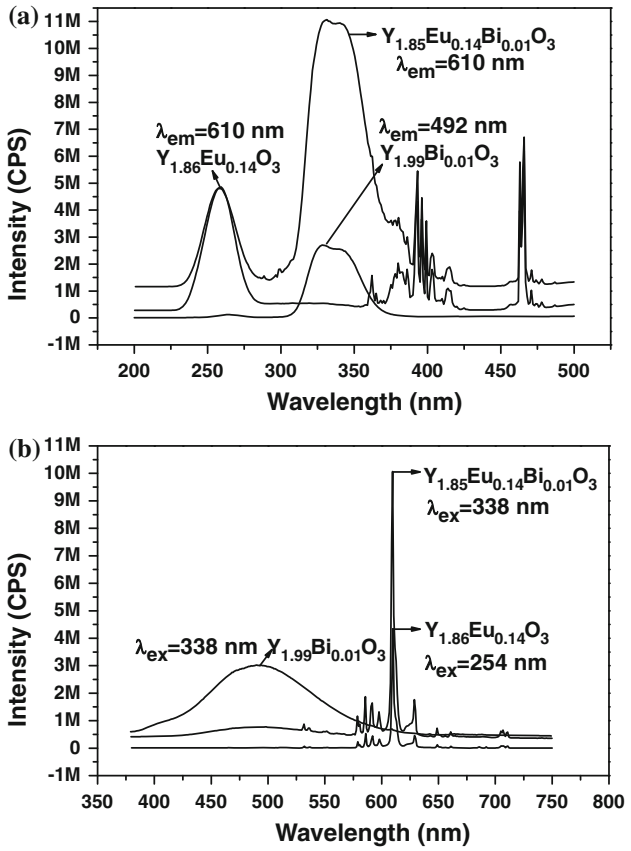

Fig. 3 PL spectra of $Y_{1.86}Eu_{0.14}O_3$, $Y_{1.99}Bi_{0.01}O_3$, and $Y_{1.85}Eu_{0.14}Bi_{0.01}O_3$ samples prepared under the same condition. **a** Excitation spectra and **b** emission spectra

Nevertheless, the particles will grow anisotropy and form special morphology as interface reaction mechanism is the dominant growth mechanism. In the MSS method, the particles form and grow through liquid transmission which has high liquidity and proliferation rate, so interface reaction mechanism is the main controlled mechanism in this method and special morphology of sample is produced.

Figure 3a and b exhibit the excitation and emission spectra of as-prepared $Y_{1.86}Eu_{0.14}O_3$, $Y_{1.99}Bi_{0.01}O_3$, and $Y_{1.85}Eu_{0.14}Bi_{0.01}O_3$ products, respectively. In the Fig. 3a, the excitation spectrum of $Y_{1.86}Eu_{0.14}O_3$ reveals not only a common wide band from 230 to 280 nm centered at 254 nm, which is assigned to Eu^{3+}–O^{2-} charge-transfer state transition, but also another band between 370 and 420 nm reaching the maximum at 393 nm as well as a peak at 466 nm, which are attributed to $^7F_{0,1}$–$^5L_6$, $^7F_{0,1}$–$^5D_2$ transitions of Eu^{3+} ions, respectively [19]. It is noteworthy that the relative intensity of these two bands at 393 and 466 nm are as strong as that of common peak at 254 nm, both of which are well coincided with the emission wavelength of the blue LEDs (λ_{em} = 440–470 nm) or the UV-LEDs (λ_{em} = 350–410 nm). This good phenomenon, which is hard to be seen in the most Eu^{3+}-doped phosphors, has been explained in detail in our previous study [20]. As for $Y_{1.99}Bi_{0.01}O_3$ sample, the excitation spectrum exhibits a weak band from 250 to 280 nm peaking around 263 nm and a strong broad band in the range of 300–375 nm with a maximum at 338 nm. It is well known that Bi^{3+} ions have a $6s^2$ electronic configuration with ground state of $^1S_0$ and a $6s6p$ configuration with the excited states split into $^3P_0$, $^3P_1$, $^3P_2$, and $^1P_1$ in the order of increasing energy. According to selection rules, the transitions to $J = 1$ levels are expected to be the highest [21–23]. Therefore, the two bands peaking at 263 and 338 nm shown in the excitation spectrum of $Y_{1.99}Bi_{0.01}O_3$ sample may be ascribed to $^1S_0$–$^1P_1$ and $^1S_0$–$^3P_1$ transitions, respectively. The three characteristic excitation bands of $Y_{1.86}Eu_{0.14}O_3$ sample and the strongest excitation band of $Y_{1.99}Bi_{0.01}O_3$ sample are all shown in the excitation spectrum of $Y_{1.85}Eu_{0.14}Bi_{0.01}O_3$ product. However, the weak excitation band of $Y_{1.99}Bi_{0.01}O_3$ sample peaking at 263 nm are not presented in the excitation spectrum of $Y_{1.85}Eu_{0.14}Bi_{0.01}O_3$ product due to overlapping with the strong band of $Y_{1.86}Eu_{0.14}O_3$ from 230 to 280 nm. As shown in Fig. 3b, the emission spectrum of $Y_{1.86}Eu_{0.14}O_3$ sample represents five groups of sharp peaks from 575 to 710 nm, which are attributed to $^5D_0 \rightarrow {}^7F_J$ ($J = 0, 1, 2, 3,$ and 4) transitions of Eu^{3+} ions. The dominant peak at 610 nm is ascribed to the forced electron dipole $^5D_0 \rightarrow {}^7F_2$ transition of Eu^{3+} ions when Eu^{3+} is occupied in low symmetry site with no inversion center. A broad band between 390 and 625 nm peaking at 492 nm is observed in the emission spectrum of $Y_{1.99}Bi_{0.01}O_3$ sample. The band is originated from the $^3P_1$–$^1S_0$ transition of Bi^{3+} ions. In the emission spectrum of $Y_{1.85}Eu_{0.14}Bi_{0.01}O_3$ sample, the characteristic peaks of $Y_{1.99}Bi_{0.01}O_3$ and $Y_{1.86}Eu_{0.14}O_3$ are both represented under the excitation wavelength of 338 nm. It is interesting that the relative intensity of peak at 610 nm is about twice stronger than that of peak at 610 nm for $Y_{1.86}Eu_{0.14}O_3$ sample, but the relative intensity of band around 492 nm reduces significantly after co-doping Eu^{3+} ions in matrix. It means that a significant energy transfer has happened between Bi^{3+} and Eu^{3+} ions and the Bi^{3+} ion plays not only as a luminescence activator but also as a sensitizer for Eu^{3+} ion in the $Y_{1.85}Eu_{0.14}Bi_{0.01}O_3$ sample. The effect of Eu^{3+} and Bi^{3+} concentrations on the relative emission intensity of $Y_{2-2x}Eu_{2x}O_3$ and $Y_{2-2y}Bi_{2y}O_3$ is displayed in Fig. 4. With increasing Eu^{3+} concentration, the relative intensity of 610 nm emission increases dramatically and reaches to the maximum at 7 mol%. While further rising Eu^{3+} concentration over 7 mol%, the intensity of red emission decreases inversely due to concentration quenching. So in the below, the content of Eu^{3+} ions is fixed at 7 mol%. The Bi^{3+} concentration has a similar influence in the relative

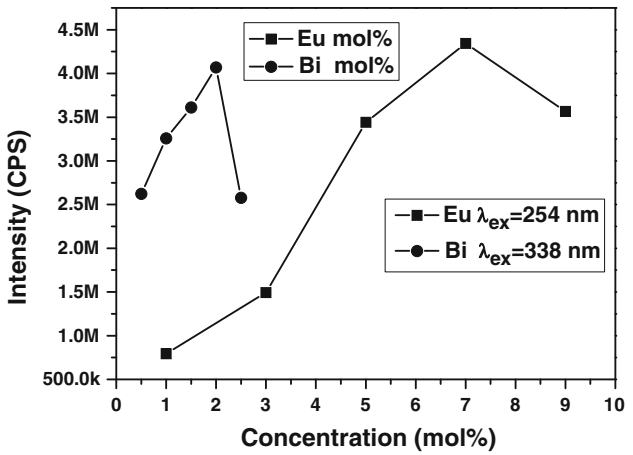

Fig. 4 Relative emission intensity of $Y_{2-2x}Eu_{2x}O_3$ (peak at 610 nm) and $Y_{2-2y}Bi_{2y}O_3$ (peak at 492 nm) as a function of Eu^{3+} and Bi^{3+} concentrations

intensity of 492 nm emission for $Y_{2-2y}Bi_{2y}O_3$ and the optimal concentration is 2 mol%.

Figure 5 shows the excitation and emission spectra of $Y_{1.86-2y}Eu_{0.14}Bi_{2y}O_3$ products varied with Bi^{3+} contents ($\lambda_{em} = 610$ nm, $\lambda_{ex} = 338$ nm, $y = 0.005$, 0.010, 0.015, 0.020, and 0.025). From Fig. 5a and b, it is obvious that five $Y_{1.86-2y}Eu_{0.14}Bi_{2y}O_3$ samples present the similar characteristic excitation, emission peaks, and variation tendency with the change of Bi^{3+} contents. With the increase of Bi^{3+} concentrations, the relative excitation and emission intensity of $Y_{1.86-2y}Eu_{0.14}Bi_{2y}O_3$ rise rapidly and get to a maximum at 1.5 mol%. Above this concentration, the intensity declines. It proves again that the energy transfer from Bi^{3+} to Eu^{3+} is happened in Y_2O_3:Eu, Bi. Meanwhile, the optimal Bi^{3+} concentration of $Y_{1.86-2y}Eu_{0.14}Bi_{2y}O_3$ is not consistent with that of 2 mol% Bi^{3+} in $Y_{2-2y}Bi_{2y}O_3$. It may be assigned to the formation of Bi^{3+} aggregations in high Bi^{3+} concentration of $Y_{1.86-2y}Eu_{0.14}Bi_{2y}O_3$. The aggregations play a role of trapping centers and distribute the absorbed energy nonradiatively instead of transferring it to Eu^{3+} ions [24].

Figure 6 shows the excitation spectrum of $Y_{1.86}Eu_{0.14}O_3$ sample under 610 nm emission and the emission spectrum of $Y_{1.99}Bi_{0.01}O_3$ sample monitored by 338 nm. From this figure, it is apparent that the emission spectrum of $Y_{1.99}Bi_{0.01}O_3$ is overlapped with the excitation band of $Y_{1.86}Eu_{0.14}O_3$ ranging from 380 to 500 nm. Therefore, It can be learned that the energy transfer from Bi^{3+} to Eu^{3+} in $Y_{1.86-2y}Eu_{0.14}Bi_{2y}O_3$ is due to the overlap between excitation band of Eu^{3+} and emission band of Bi^{3+}. The concrete energy transfer processes between Bi^{3+} and Eu^{3+} in $Y_{1.86-2y}Eu_{0.14}Bi_{2y}O_3$ and corresponding luminescence mechanism are presented in Fig. 7. First, when $Y_{1.86-2y}Eu_{0.14}Bi_{2y}O_3$ phosphor is excited by 338 nm, the Bi^{3+} ions would absorb the excitation energy of 338 nm.

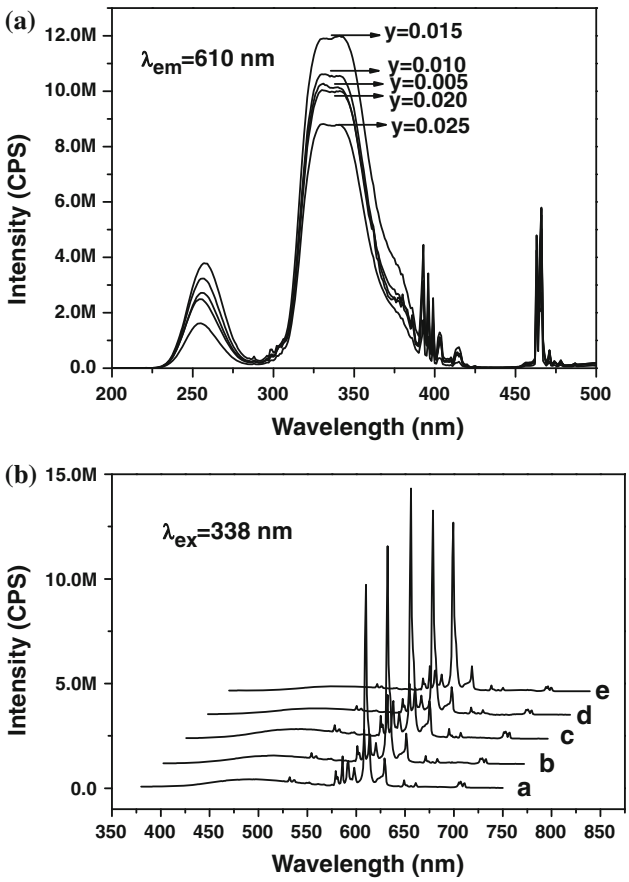

Fig. 5 PL spectra of $Y_{1.86-2y}Eu_{0.14}Bi_{2y}O_3$ samples with respect to Bi^{3+} concentrations. **a** Excitation spectra, **b** emission spectra, *a*: $y = 0.005$, *b*: $y = 0.010$, *c*: $y = 0.015$, *d*: $y = 0.020$, and *e*: $y = 0.025$

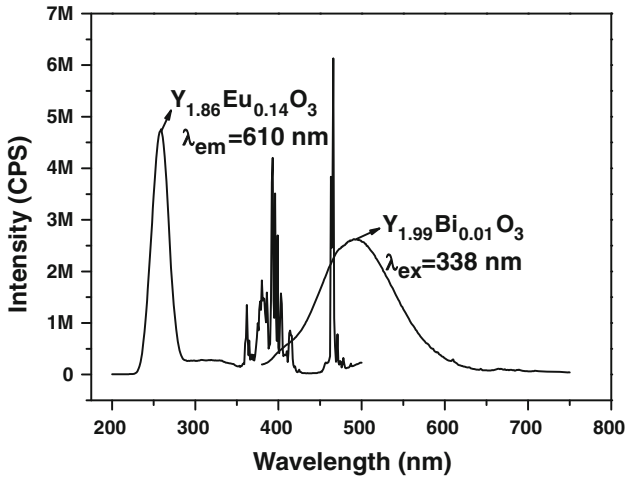

Fig. 6 Excitation spectrum of $Y_{1.86}Eu_{0.14}O_3$ sample ($\lambda_{em} = 610$ nm) and emission spectrum of $Y_{1.99}Bi_{0.01}O_3$ sample ($\lambda_{ex} = 338$ nm)

Second, the excited Bi^{3+} ions release the energy non-radiatively to Eu^{3+} ions, which makes Eu^{3+} ions take place $^7F_{0,1}$–$^5L_6$, $^7F_{0,1}$–$^5D_2$ transitions. Finally, the excited Eu^{3+}

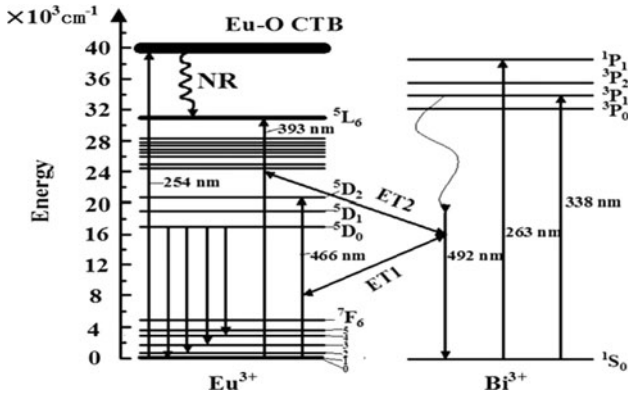

Fig. 7 The luminescence and energy transfer process of Eu^{3+} and Bi^{3+} in $Y_{1.86-2y}Eu_{0.14}Bi_{2y}O_3$

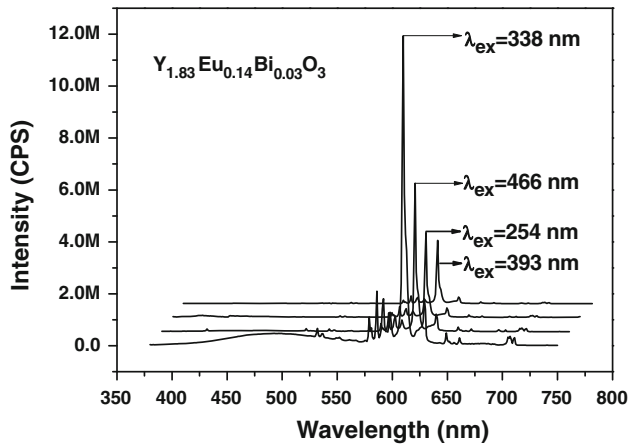

Fig. 8 Emission spectra of $Y_{1.83}Eu_{0.14}Bi_{0.03}O_3$ varied with excitation wavelengths

ions emit red light by $^5D_0 \rightarrow {}^7F_J$ ($J = 0$, 1, 2, 3, and 4) transitions.

Figure 8 represents the emission spectra of $Y_{1.83}Eu_{0.14}Bi_{0.03}O_3$ excited by 254, 338, 393, and 466 nm, respectively. All spectra exhibit good characteristic emission of Eu^{3+} ions and also show blue emission of Bi^{3+} ions as monitored by 338 nm. Combining Fig. 3 with Fig. 8, it can be learned that Eu^{3+} and Bi^{3+} co-doped Y_2O_3 red phosphors prepared by MSS method are able to be excited by not only 254 and 466 nm but also the light in the range of 330–420 nm, which are in well agreement with the requirements of white LEDs for red phosphors. The comparison of emission spectra of $Y_{1.83}Eu_{0.14}Bi_{0.03}O_3$ prepared by MSS with that of $Y_{1.83}Eu_{0.14}Bi_{0.03}O_3$ and $Y_{1.86}Eu_{0.14}O_3$ fabricated by SSR is shown in Fig. 9. Due to the addition of Bi^{3+} ions, the dominant peaks of $Y_{1.83}Eu_{0.14}Bi_{0.03}O_3$ for MSS and SSR are both located about 338 nm. So 338 nm is fixed as excitation wavelength in Fig. 9. It is explicit that three profiles exhibit similar characteristic emission of Eu^{3+} ions. Furthermore, the relative emission intensity of

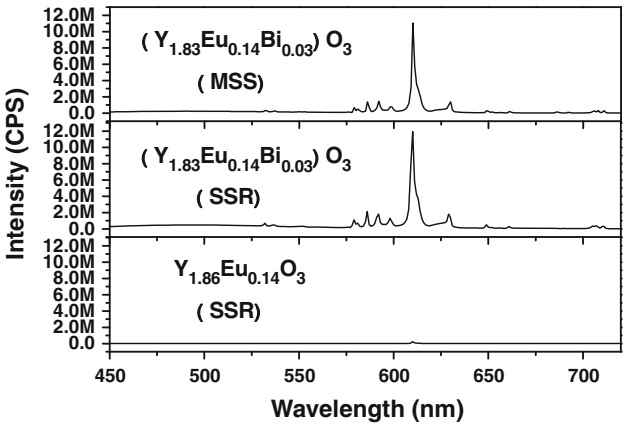

Fig. 9 Emission spectra of $Y_{1.83}Eu_{0.14}Bi_{0.03}O_3$ prepared by MSS and $Y_{1.83}Eu_{0.14}Bi_{0.03}O_3$, $Y_{1.86}Eu_{0.14}O_3$ synthesized by SSR monitored under 338 nm

as-prepared $Y_{1.83}Eu_{0.14}Bi_{0.03}O_3$ by MSS is as strong as that of $Y_{1.83}Eu_{0.14}Bi_{0.03}O_3$ obtained by SSR but much higher than that of $Y_{1.86}Eu_{0.14}O_3$ synthesized by SSR owing to the absence of Bi^{3+} ions in $Y_{1.86}Eu_{0.14}O_3$. It means that compared with Y_2O_3:Eu, Bi fabricated by SSR, the as-expected Y_2O_3:Eu, Bi not only can be synthesized at a much lower temperature (550 °C) via MSS but also has similar emission intensity. Based on these results, we can know that the as-obtained Y_2O_3:Eu, Bi red phosphors by MSS in our study would have a promising application in the area of white LEDs.

Conclusions

$Y_{1.86-2y}Eu_{0.14}Bi_{2y}O_3$ (y: 0–0.025) phosphors were successfully prepared by MSS method at a low temperature. According to XRD and SEM results, these phosphors represent good cubic crystallinity and octahedral morphology with smooth surface as well as relatively uniform particle size. With increasing Bi^{3+} concentration, luminescence intensity of the phosphors rise significantly via energy transfer between Bi^{3+} and Eu^{3+} ions and the optimal concentration of Bi^{3+} ions is 1.5 mol%. The as-prepared red phosphors by MSS method not only can be excited by 254, 466 nm and the light in the range of 330–420 nm but also emit similar intensity of red light as that of sample obtained by conventional SSR. Therefore, the phosphor fabricated by MSS method in our study will be a promising red phosphor in the field of white LEDs.

Acknowledgements This study was supported by the Fundamental Research Funds for the Central Universities (No. CUG090108) and Guangdong Province Enterprise-University-Academy Collaborative Project (No. 2010B090400437).

References

1. Kim JS, Jeon PE, Choi JC, Park HL, Mho SI, Kim GC (2004) Appl Phys Lett 84:2931
2. Hu Y, Zhuang W, Ye H, Zhang S, Fang Y, Huang X (2005) J Lumin 111:139
3. Mueller AH, Petruska MA, Achermann M, Werder DJ, Akhadov EA, Koleske DD, Hoffbauer MA, Klimov VI (2005) Nanoletters 5:1039
4. Narendran N, Gu Y, Freyssinier-Nova JP, Zhu Y (2005) Phys Status Solidi (a) 202:R60
5. Li YQ, Delsing AC, De With G, Hintzen HT (2005) Chem Mater 17:3242
6. Wang Y, Sun Y, Zhang J, Ci Z, Zhang Z, Wang L (2008) Physica B 403:2071
7. Zhao X, Wang X, Chen B, Meng Q, Di W, Ren G, Yang Y (2007) J Alloys Compd 433:352
8. Nakamura S, Fasol G (1997) The blue laser diodes, GaN based light emitters and lasers. Springer, Berlin
9. Thomas M, Rao PP, Deepa M, Chandran MR, Koshy P (2009) J Solid State Chem 182:203
10. Hu Y, Zhuang W, Ye H, Wang D, Zhang S, Huang X (2005) J Alloys Compd 390:226
11. Cao F, Tian Y, Chen Y, Xiao L, Liu Y, Li L (2009) Mater Sci Semicond Process 12:94
12. Neeraj S, Kijima N, Cheetham AK (2004) Chem Phys Lett 387:2
13. Strel'tsov AV, Dmitrienko VP, Akmaeva TA, Kudryavtsev SV, Dmitrienko AO, Razumov KA (2009) Inorg Mater 45:889
14. Chi LS, Liu RS, Lee BJ (2005) J Electrochem Soc 152:J93
15. Park WJ, Yoon SG, Yoon DH (2006) J Electroceram 17:41
16. Chan T-S, Kang C-C, Liu R-S, Chen L, Liu X-N, Ding J-J, Bao J, Gao C (2007) J Comb Chem 9:343
17. Guo P, Zhao F, Guobao L, Liao F, Tian S, Jing X (2003) J Lumin 105:61
18. Cahn JW (1967) In: Peiser HS (ed) Crystal growth. Pergamon, Oxford
19. Bazzi R, Flores MA, Louis C, Lebbou K, Zhang W, Dujardin C, Roux S, Mercier B, Ledoux G, Bernstein E, Perriat P, Tillement O (2004) J Colloid Interface Sci 273:191
20. Wu X, Liang Y, Liu R, Li Y (2010) Mater Res Bull 45:594
21. Fukada H, Konagai M, Ueda K, Miyata T, Minami T (2009) Thin Solid Films 517:6054
22. Porter-Chapman Y, Bourret-Courchesne E, Derenzo SE (2008) J Lumin 128:87
23. Liu G, Zhang Y, Yin J, Zhang WF (2008) J Lumin 128:2008
24. Park WJ, Jung MK, Yoon DH (2007) Sens Actuators B 126:324